An improved thermodynamic model of metal-olivine-pyroxene stability domains

J. Matas[1,a], Y. Ricard[1], L. Lemelle[2,b] and F. Guyot[2]

[1] École normale supérieure de Lyon, UMR/CNRS 5570, Lyon, France.

[2] Laboratoire de Minéralogie-Cristallographie, Institut de Physique du Globe, Paris, France.

[a] present address: Department of Geology and Geophysics, University of California, Berkeley.

[b] present address: École normale supérieure de Lyon, UMR/CNRS 5570, Lyon, France.

e-mail address: jmatas @ ens-lyon.fr

fax: 1-510-643-9980

Abstract

Interactions between several silicate and metallic phases are studied by applying a selfconsistent thermodynamic approach and using the recent relevant thermodynamic data. We compute proportions and compositions of oxidized silicates and of reduced metallic phase in equilibrium at various temperatures and oxygen fugacities. The empirically observed activity-composition relationships for ternary metallic alloys are used and their applications to a general thermodynamic expression for a non-regular ternary system is explicitly discussed. We show that the stability limits of olivines and pyroxenes with respect to precipitation of metallic phases under reducing conditions are directly related to the presence of nickel impurities. We precisely evaluate the modifications of the stability limits as a function of nickel content. For typical mantle olivines (Fe/(Fe+Mg)=0.1) the stability limits are given for values of x_{Ni}=Ni/(Ni+Fe+Mg) ranging from 10 ppm to 1% by: $\ln f_{O_2} = -39.83 + 7.86 \ln x_{Ni}$, $\ln f_{O_2} = -14.68 + 6.21 \ln x_{Ni}$, at 900 K and 1600 K, respectively.

Introduction

Olivine is the major mineral of the Earth's upper mantle; a precise knowledge of its stability field is therefore important, especially for understanding laboratory measurements performed on this mineral. This stability domain not only depends on pressure and temperature but also on oxygen fugacity, f_{O_2}, e.g. Nitsan (1974). At low enough oxygen fugacities, metallic iron is extracted from forsterite-fayalite solid-solutions as predicted (Nitsan 1974) and experimentally observed (Boland and Duba 1981; Boland and Duba 1986; Lemelle et al. 1999). In addition to its potential importance for core formation in the Earth, this phenomenon might explain some characteristics of olivine-metal interactions in meteorites (e.g. dusty olivines). The observation of Elligham diagrams suggests that the presence of minor components can significantly modify the olivine stability field with respect to oxygen fugacity. The purpose of this paper is to present a precise computation method for calculating the stability limit of natural olivines with respect to oxygen fugacity, taking into account the presence of minor components. We compute the stability limit under reducing conditions of mantle olivines modeled as a solid solution of forsterite (Mg_2SiO_4) and fayalite (Fe_2SiO_4) containing nickel as a major impurity. Similar calculations were performed by Arculus et al. (1990); in this study, we extend their approach using a free-energy minimization procedure with updated thermodynamic data. In particular, this method allows us to take into account non-ideal activity-composition relationships for minor elements such as silicon in the metallic phase. The solubility of silicon in metal can become important at very low oxygen fugacities and this phenomenon can have important implications to enstatite chondrites and possibly to early Earth.

Calculation procedure

All the computations are performed within the temperature range 700K-2100K at 1 bar total pressure. Under these temperature and pressure conditions, precise thermodynamic data can be used. The involved phases are olivine (Mg_2SiO_4, Fe_2SiO_4, Ni_2SiO_4 endmembers), orthopyroxene ($MgSiO_3$, $FeSiO_3$, $NiSiO_3$), quartz α, β and cristobalite (SiO_2), metal (Fe, Ni, Si) with bcc and fcc structures and oxygen (O_2). As discussed below, some results at the highest temperatures are indeed obtained in the stability field of molten silicates or metal, and the corresponding calculations are therefore metastable extrapolations. Thermodynamic data for the endmembers are summarized in Tables 1a and 1b. The values of enthalpy of formation ΔH_0 has been modified for three components: fayalite (+0.5 kJ/mol), ferrosilite (-0.5 kJ/mol), and cristobalite (+1 kJ/mol). This modification was needed to reconcile both thermodynamic simulations and experimental observations (Bowen and Schairer 1935; Smith 1971; Wood and Strens 1971) of equilibrium between ferrosilite and fayalite + SiO_2-phases. We note that all these corrections are smaller than uncertainties on measured values of enthalpy. **To our knowledge, no thermodynamic data are available for the $NiSiO_3$ orthopyroxene endmember. We therefore estimated its thermodynamic properties using the approach developped by Helgeson et al. (1978) and Sverjensky (1984). Estimated values of enthalpy of formation ΔH_0 and of entropy S_0 are listed in Table 1a. The heat capacity of $NiSiO_3$ equals the sum of heat capacities of NiO and SiO_2 (Helgeson et al. 1978).** The uncertainties introduced by these assumptions are discussed later. The solid solutions are modeled by standard methods. The chemical potential μ_i of each endmember i of a solid solution is given by

$$\mu_i = \mu_i^0(T,P) + RT \ln a_i \,, \tag{1}$$

where the activity-composition relations are given by:

$$RT \ln a_i = sRT \ln x_i + sRT \ln \gamma_i \,, \tag{2}$$

where s is **the crystallographic site multiplicity (Spear 1993)** and x_i is t he molar fraction. For olivine endmembers, s=2; for orthopyroxene, oxide, and metal endmembers, s=1. The complexity comes from the activity coefficients γ_i. These coefficients are functions of temperature, pressure and concentrations in the solid solution. They are determined from experiments and then, for practical use, fitted with simple functions. However, the Gibbs-Duhem condition implies a relation between the activities of the endmembers in a given solid solution:

$$\sum_i x_i d \ln a_i = 0 \,. \tag{3}$$

In this paper we deal at most with ternary solutions. In these cases, a general expression for the activity coefficients is given by a non-regular ternary Margules expansion (Helffrich and Wood 1989; Spear 1993),

$$RT \ln \gamma_i = 2W_{ji} x_i x_j (1 - x_i) + W_{ij}(x_j^2 - 2x_i x_j^2) + 2W_{ki} x_i x_k (1 - x_i)$$

$$+W_{ik}(x_k^2 - 2x_i x_k^2) - 2W_{kj} x_j^2 x_k - 2W_{jk} x_j x_k^2 + W_0(x_j x_k - 2x_i x_j x_k) \,, \tag{4a}$$

where the end members have indices i,j and k, and where

$$W_0 = \frac{1}{2}(W_{ij} + W_{ji} + W_{ik} + W_{ki} + W_{jk} + W_{kj}) - C_{ijk} \,. \tag{4b}$$

This expression is consistent with the Gibbs-Duhem condition for any set of interaction energies or Margules parameters, W, and any possible ternary excess term C_{ijk}.

In olivine and orthopyroxene the reference states are the pure endmembers (Mg_2SiO_4, Fe_2SiO_4, Ni_2SiO_4), ($MgSiO_3$, $FeSiO_3$, $NiSiO_3$), respectively. When our computations are restricted to binary

solutions (in the absence of Ni), the expression of the activity coefficient (4a) is drastically simplified and becomes:

$$RTln\gamma_i = W_{ij}(1 - x_i)^2 \,, \tag{5}$$

assuming a regular symmetric mixing model ($W_{ij} = W_{ji}$). This approximation is justified by the quantity and precision of available activity-composition measurements in this system. We also adopted a regular symmetric mixing model in Mg-Fe-Ni ternary olivines and orthopyroxenes. In this case expression (4a) reduces to:

$$RT \ln \gamma_i = W_{ij}x_j^2 + W_{ik}x_k^2 + (W_{ij} + W_{ik} - W_{jk})x_j x_k \,. \tag{6}$$

As $W_{ij} = W_{ji}$ for each i and j, only 3 interaction energies are required, and are given in Table 2a. For oxides, we assumed an ideal solution and we did not search for more precise activities as it is experimentally known that no oxides should be formed under the conditions of our computations.

The problem of activity-composition relations is more complicated in the case of metallic alloys, in particular because of the highly non-ideal behavior of silicon in metallic iron. There only available expertise comes from metallurgy, e.g. Rist et al. (1974); Schwerdtfeger and Engell (1964); Chart (1970); The Japan Society for the Promotion of Science (1981). Metallurgy literature (McCoy et al. (1967); Gaskell (1981); Nash and Nash (1991); Raghavan (1989)) adopts a solution formalism, considering iron as the solvent (reference state pure Fe), and silicon Si and/or nickel as solutes (reference states Ni and Si at infinite dilution in Fe). The activity-composition relations are written (Rist et al. 1974);

$$RT \ln a_i^{Fe} = \Delta G_i^{Fe}(T) + RT \ln f_i^{Fe} p_i \,, \tag{7}$$

where $\Delta G_i^{Fe}(T)$ is the enthalpy of dissolution of the solute i (e.g. Ni or Si) in Fe (Table 2b). Instead of molar fractions, weight percentages (wt%) of the solute i in the alloy, p_i are used in metallurgy. In (7), f_i^{Fe} is an appropriate activity coefficient. The requirement that f_i^{Fe} is 1 at infinite dilution implies a first order expansion of the activity coefficient f_i^{Fe} in the following form:

$$\ln f_i^{Fe} = \sum_{j=solute} e_{i/j}^{Fe} p_j \,. \tag{8}$$

Some coefficients of interaction $e_{i/j}^k$ (for example, the coefficient $e_{Ni/Ni}^{Fe}$ which characterizes the interaction of Ni with itself when diluted in Fe) are experimentally determined (Rist et al. 1974). The enthalpy of dissolution, $\Delta G_{Si}^{Ni}(T)$, of Si in Ni considered as the solvent is also available as well as two coefficients of interaction $e_{Si/Si}^{Ni}$ and $e_{Fe/Fe}^{Ni}$ (Witzke and Gatellier 1996). Due to the paucity of solution data in solid iron, we use the $e_{i/j}^k$ parameters in liquid iron at 1 bar and 1873 K (Table 2c).

It should be noted that expression (8) only holds when the molar fractions of Si and Ni in the alloy do not exceed x_i=0.25. If the concentration of nickel or silicon is close to 1, both chemical activity a_i and activity coefficient γ_i must be equal to 1. This necessary condition is not fulfilled by (7-8) which is not surprising as these equations have been established for metallurgy assuming very large dilutions. For our purpose, we would like to have activity-composition relations also valid for higher Si and Ni concentrations. Another problem in applying the metallurgical approach to geophysics is that we cannot use the equations (7-8) and assume at the same time that the iron behaves ideally; this would not satisfy the Gibbs-Duhem condition (3). Furthermore, it can be mathematically shown that no activity can be found for iron satisfying exactly the condition (3) when the two solute activities are given by (7-8). What has been done was to identify the Taylor expansion of the theoretical expression (4a) with that of the empirical model (7-8) (see Appendix). This allows us to deduce the 7 corresponding Margules coefficients W_{ij}. **Because of RT term and the temperature dependent enthalpies of dissolution (see equations (A5)-(A7)) the coefficients W_{ij} turn out temperature de-**

pendent. The appropriate values are listed in Table 2d for three different temperatures T=1273, 1573, and 1873 K. One can notice that they vary almost linearly and, thus, we also listed their temperature derivatives. Our approach allows us to compute activities valid for any composition of the ternary system verifying the Gibbs-Duhem condition and agreeing with available experimental results. However, we do not consider any ordered phases, such as FeSi, Fe_2Si, or $FeNi_3$, see e.g., Raghavan (1989). This approximation is justified by the fact that we only deal with ternary alloys containing small amount of silicon and compute the equilibrium composition at high temperatures outside of the stability domain of $FeNi_3$. The activities predicted in a hypothetical ternary Fe-Ni-Si alloy are depicted in Fig 1. For each endmember, Si, Ni, and Fe, the activity is shown using a triangular representation. Activities are 1 (the darkest shading) for a pure solvent and are 0 for an infinitely diluted solute. If the ternary system were ideal, the isoactivity lines of Si, Ni and Fe would be equidistant and parallel to the side opposite to the corner labeled with their names. **These diagrams indicate that 1) the Fe-Si-Ni alloy is an asymmetric solution and that Si is highly non-ideal. Due to the nonideal mixing (the Margules's parameters are not zero) the chemical potential of metallic silicon becomes more negative and, thus, its solubility in a Fe-Ni significantly increases.** The Fe-Ni behavior is more ideal, unless Si is present.

Results

Having defined the activity-composition relationships we can now apply our numerical code to compute silicate-metal equilibrium as a function of temperature. In this paper we concentrate on 1 bar metal-silicate equilibrium and mainly discuss experimental implications. A high-pressure extension having important implications for the early Earth evolution will be treated in a forthcoming

paper. Moreover, this extension needs good quality high-pressure data which are not available for some phases, especially for Ni-bearing silicates.

Stability limits of binary Fe-Mg olivine and orthopyroxene solid solutions

We start with simple mineralogical solutions and compute the stability limits of Fe_2SiO_4 fayalite (Fa) and $FeSiO_3$ ferrosilite (Fs) with respect to reduction, in order to compare our results with those of Nitsan (1974). In this case, an analytical solution can be found. The chemical reactions to be studied are:

$$\mathrm{Fe}_\alpha\mathrm{SiO}_\beta \rightleftharpoons \alpha\mathrm{Fe} + \mathrm{SiO}_2 + (\frac{\beta}{2} - 1)\mathrm{O}_2\,, \tag{9}$$

where α and β are appropriate stoichiometric coefficients. At equilibrium, the previous equation implies that the oxygen fugacity f_{O_2} is given by

$$(\frac{\beta}{2} - 1)RT \ln f_{\mathrm{O}_2} = \mu_{\mathrm{Fe-silicate}} - \alpha\mu_{\mathrm{Fe}} - \mu^0_{\mathrm{silica}} - (\frac{\beta}{2} - 1)\mu^0_{\mathrm{oxygen}}\,. \tag{10}$$

In the simplest case where only iron is present in metal and no magnesium is present in silicate, the chemical potentials μ_i are simply the standard potentials μ_i^0. The reaction is univariant and the only equilibrium line corresponds to a relation between temperature and oxygen fugacity.

In more realistic cases where both silicate and metal are solid state solutions, their chemical potentials are given by equation (1). Let us consider first, the possible dissolution of silicon in the metallic phase. The reaction

$$\mathrm{SiO}_2 \rightleftharpoons \mathrm{Si}_{\mathrm{metal}} + \mathrm{O}_2 \tag{11}$$

must therefore be considered together with (9). The equilibrium remains univariant as one species (Si_{metal}) and one independent chemical relation (11) have been added to the system. In this case, by combining (9) and (11) one finds that the concentration of silicon in the metallic phase is fixed at a given temperature, and given by

$$RT \ln\left(\frac{a_{Fe}^{\alpha}}{a_{Si}^{\beta/2-1}}\right) = \mu^0_{Fe-silicate} + \left(\frac{\beta}{2} - 1\right)\mu^0_{Si} - \alpha\mu^0_{Fe} - \frac{\beta}{2}\mu^0_{silica}\,. \qquad (12)$$

Solving (12) using (2) and (4) allows us to compute the iron activity in metal and then the potential μ_{Fe}. As the chemical potential of silicates remains standard, we readily obtain the oxygen fugacity f_{O_2} using (10). Following the notations used in Nitsan (1974), we call OSI the stability limit of pure fayalite under reducing conditions in the system olivine-silica-iron (α=2, β=4). Similarly the PSI curve stands for the equilibrium in the system pyroxene-silica-iron (α=1, β=3).

Fig. 2a and 2b depict the OSI and PSI stability curves in the ($1/T$, f_{O_2}) space with their associated uncertainties (shaded areas) obtained, here and in the following curves, by varying the thermodynamic parameters within the error bars associated to the relevant measurement. For comparison the curves given by Nitsan (1974) are also shown as dashed lines. The results are generally in good agreement, although significant discrepancies are observed below 900 K. These discrepancies are due to differences in the endmember thermodynamic data, and not to details of the activity model; very small amounts of silicon dissolve in iron resulting in iron activity remaining close to 1. The amount of silicon dissolved in the metallic phase in equilibrium with fayalite or ferrosilite depends on temperature, varying from less than 10−9 wt% below 1000 K, to 10^{-5} wt% at the melting point of the silicates.

Depending on the temperature range, we used thermodynamic data for the stable phases of metal (bcc or fcc) and silica (α-quartz, β-quartz or cristobalite). The stability domains are indicated in Fig. 2. The free-energy difference between quartz and cristobalite yields shifts of the stability curve by less than 0.1 f_{O_2} log-units, which is within the errors due to combined uncertainties on thermodynamic

parameters. Differences between α and β-quartz and cristobalite and tridymite (not considered) are even more negligible. Pure Fe metal changes from a bcc to fcc structure at 1185 K and transforms back to a bcc structure above 1667 K. The free energy difference between the two forms of Fe has been computed by Guillermet and Gustafson (1985), and has a negligible effect on the stability limit. Above 1490, 1413, 1811 K for fayalite, ferrosilite and metal, respectively, the phases are molten; the calculations above these temperatures are simply metastable extensions; in these domains, the real stability limit might be quite different from that computed here, although it can be safely inferred that they will remain close to the metastable extensions up to 100 K above melting point. The OSI and PSI stability limits with respect to reduction are shown in Fig. 3a and 3b for three different olivine compositions (Fa100-pure fayalite, Fa10-$(Mg_{0.9}Fe_{0.1})_2SiO_4$, Fa1-$(Mg_{0.99}Fe_{0.01})_2SiO_4$) and three different ortho-pyroxene compositions (Fs100-pure ferrosilite, Fs10-$Mg_{0.9}Fe_{0.1}SiO_3$ and Fs1-$Mg_{0.99}Fe_{0.01}SiO_3$). The effect of the iron dilution by magnesium in olivine and orthopyroxene is to expand the stability fields toward more reducing conditions. If we neglect non-ideal mixing in olivine and orthopyroxene and assume γ_{Fe}=1, the PSI and OSI stability boundaries shift towards even more reducing conditions (dashed lines). The difference between non-ideal and ideal mixing models is larger than thermodynamic uncertainties (shaded areas) in the case of OSI. The destabilization reaction of a fayalite-forsterite solid solution under reducing conditions does not necessarily yield olivine-silica-iron assemblages (OSI). If the OSI boundary curve occurs at more oxidizing conditions than PSI, an olivine-orthopyroxene-iron (OPI) assemblage is formed, according to:

$$Fe_2SiO_4 \rightleftharpoons Fe + FeSiO_3 + \frac{1}{2}O_2\,. \tag{13}$$

In the case where Mg is absent it is easy to write equivalents of equations (10) and (12) and compute the OPI stability curve. **When Mg is present, both activities of fayalite and ferrosilite become related to the ratios Mg/Fe in olivine and pyroxene. The latter are unknown**

variables in equations equivalent to (10) and (12) and to solve such problem analytically would be cumbersome. Therefore, we developed a numerical code, minimizing the Gibbs free energy of a chemical system subject to element abundance constrains. The numerical method uses a stoichiometric formulation of the minimization problem adapted from Smith and Missen (1991). The results are the molar abundances of the different endmembers in each coexisting phase, as a function of pressure and temperature, assuming thermodynamic equilibrium. The input parameters are (1) the bulk chemical composition of the system, (2) a list of all possible phases and components involved in the system, (3) the standard chemical potentials of the endmembers at all investigated P and T and 4) the activity-composition models for each solid solution. **For each free-energy minimization, oxygen fugacity is calculated by using one or several chemical equilibria involving oxygen, a posteriori. When the total amount of oxygen n_{O} in the system equals the quantity of oxygen n_{O}^{*} needed to obtain fully oxidized system,**

$$n_{\mathrm{O}}^{*} = n_{\mathrm{Mg}} + n_{\mathrm{Fe}} + n_{\mathrm{Ni}} + 2n_{\mathrm{Si}}\,,$$

no metallic phase is present. The oxygen fugacity is, however, defined by an chemical equilibrium between an oxidized and reduced phase, i.e. when $n_{\mathrm{O}} \rightarrow n_{\mathrm{O}}^{*}$. Thus, to obtain the stability limit of a given silicate we lower the quantity of oxygen corresponding to its stoichiometry by an infinitesimal amount and compute the corresponding oxygen fugacity.

Starting from olivine, our program automatically chooses the appropriate equilibrium (OPI or OSI) that leads to the minimum free energy. The OPI curve is found to be very close to OSI, and we plot the difference between these two curves as a function of temperature in Fig. 4. Assuming that the silicon concentration in the metallic phase is small, these differences can also be understood in terms of an equivalent silica activity ($\ln a_{\mathrm{SiO_2}} = \ln f_{\mathrm{O_2}}^{\mathrm{OSI}} - \ln f_{\mathrm{O_2}}^{\mathrm{OPI}}$). For magnesium-rich compositions,

the OPI rather than OSI reaction occurs, at least at low temperatures. This indicates that the olivine destabilization at reducing condition leads to pyroxene-metal assemblages. For iron-rich compositions, uncertainties in endmember thermodynamic parameters cause large uncertainties on silica activity and prevent a precise determination of whether olivines destabilize according to OPI or to OSI. The only constrains come from experimental observations on stability of iron-rich orthopyroxene by Bowen and Schairer (1935, Smith (1971, Wood and Strens (1971). The latter indicate that ferrosilite ($FeSiO_3$) decomposes into fayalite + silica at room pressure and all temperatures which is in agreement with our predictions.

The iron dilution by magnesium in olivine or orthopyroxene causes an increase of the still small amount of silicon present in the metallic phase at OPI and PSI equilibria (Fig. 5). At a temperature of about 1800 K and for a silicate with a Fe/(Fe+Mg) molar ratio of 10%, the concentration of Si in the alloy is $4x10^{-3}$ wt%. **We note that possible point defects in silicates are not considered here. Nakamura and Schmalried (1983) have shown that cation vacancies in fayalite can yield an exsolution of FeO and SiO_2 phases. They concluded, however, that the non stoichiometry of olivine drops almost exponentially with the fraction of Mg in solid solution. They have also shown that the concentration of cation vacancies decreases at very low oxygen fugacities. It is obvious that for a precise modeling of silicon concentration in metallic alloy one should include effect of nonstoichiometry. Due to the absence of thermodynamic parameters of such compounds we are, however, unable to include this phenomenon into our model.**

Stability field of mantle olivine and composition of metal and silicate phases in thermodynamic equilibrium

The main difference between a mantle olivine and a fayalite-forsterite solid solution is the presence of nickel as a major impurity. Other impurities are present (e.g. Ca, Mn, Cr), but they are less important, as far as metal precipitation is concerned, and they will be neglected here. San Carlos olivine containing about 3000 wtppm of Ni_2SiO_4 (O'Neill 1991) is used as a model for the mantle olivine and is approximated by $(Mg_xFe_yNi_z)_2SiO_4$ where x=.900 y=0.098 and z=0.002. As shown in Fig. 6, its stability limit is shifted to higher f_{O_2}'s, by about 1 to 3 log f_{O_2} units in comparison with a fayalite-forsterite solid solution of equivalent composition. It is a consequence of the combined precipitation of Ni and Fe in the metallic phase. This fact should be recognized when performing experiments on natural olivines under controlled oxygen fugacity. The San Carlos olivine stability line is barely controlled by the stability of Ni_2SiO_4. As Ni is present in very small quantities, it has a quasi-ideal behavior and the stability line is independent of the non-ideal mixing coefficients. The main sources of uncertainties in the stability limit of San Carlos olivine under reducing conditions come from the endmember thermodynamic parameters. The effect of Ni on the stability limit of Fa10 olivine is given at two representative temperatures by:

$$\ln f_{O_2} = -39.83 + 7.86 \ln x_{Ni} \quad \text{at} \quad T = 900K \tag{14a}$$

$$\ln f_{O_2} = -14.68 + 6.21 \ln x_{Ni} \quad \text{at} \quad T = 1600K \tag{14b}$$

The composition of metal in equilibrium with San Carlos olivine strongly depends on temperature, as shown in Fig. 7. It shifts from almost pure nickel at low temperature to more iron-rich compositions at higher temperatures. This explains why the difference in oxygen fugacity between Ni-bearing and Ni-free olivine decreases as temperature increases (see Fig. 6). The silicon content in the metallic phase remains negligible over the whole temperature range.

As oxygen fugacity is decreased away from the stability curve, at constant temperature (T=1700 K in Fig. 8), a Ni-rich metal precipitates. As f_{O_2} further decreases, this metal becomes enriched in iron, and then in silicon at very low oxygen fugacity (shaded areas of Fig. 8a). The compositions of the olivine and pyroxene phases in equilibrium with the metal are given in Fig. 8b and 8c. As expected, at very low oxygen fugacity, the silicate compositions are close to pure forsterite and enstatite. The calculated composition of the metallic phase is very sensitive to the activity coefficient of Si in metal. **In the past works, e.g. Guyot et al. (1997), the metallic alloy has been considered as an ideal Fe-Ni-Si solid solution and the chemical potential of metallic silicon has been corrected by using a constant activity coefficient γ_{Si}. The latter was obtained by setting x_{Fe} to 1, x_{Ni} to 0 and x_{Si} to 0 in equation (4a), i.e. $RT \ln \gamma_{\mathrm{Si}} = W_{SiFe}$. As shown in Figure. 8a (dotted lines) this approximation leads to a much more Si-enriched metal at low f_{O_2} than what is predicted by using a precise formalism. Future experiments could be used to determine the actual activity-composition relations for silicon in solid metal by measuring metal compositions equilibrated at low oxygen fugacities in this system.**

It should be also noted that a real metallic alloy is molten at high temperatures and low oxygen fugacities (high Si concentrations). Considering the experimental results by Jones and Drake (1986) and Ehlers et al. (1992) we think that our solid solution model can be viewed as an limiting case. Since the partition coefficients between silicate melts and metal should be comparable or slightly lower than those predicted by solid state chemical equilibrium computations. This means, for instance, that the solubility of nickel in silicates will not increase when molten phases are present.

Stability field of a simplified model of peridotite

For computing the reducing stability limits of an upper mantle assemblage at 1 bar, we consider a simplified model of mantle bulk composition LOSIMAG inferred by Hart and Zindler (1986). In this particular model, we take the Fe/Mg and Ni/Mg ratios of 0.1120 and 0.0032, respectively, and neglect the aluminium and calcium contents. The total amount of silica is chosen in order to obtain 60 wt% of olivine and 40 wt% of pyroxene. Therefore, the following peridotite of bulk composition Mg=1.435, Fe=0.161, Ni=0.0046, Si=1, O=3.6006 (molar proportions) is considered. When the Ni content is neglected, the computed stability limit of this simplified peridotite (Fig. 9) is almost identical to that of Fa10. This is not surprising since this peridotite is indeed an assemblage of olivine Fa10 and orthopyroxene Fs10 that have very close stability limits. As shown in Fig. 9, the computed stability limit of Ni-bearing peridotite is slightly shifted to more oxidizing conditions than those of San Carlos olivine. This comes from the fact that Ni content in the upper mantle olivines (calculated from bulk composition of Hart and Zindler (1986)), appears to be on average slightly higher than in mantle olivine.

Conclusions

In this study we have presented a thermodynamic approach which can be used for computing stability domains in olivine-pyroxene-metal systems. Using the free-energy minimization we computed equilibrium compositions of various phases as a function of temperature and oxygen fugacity. Particularly, the composition of ternary Fe-Ni-Si metallic alloy was studied using metallurgical measurements of activity-composition relationships. Usually the presence of silicon in metallic phase is neglected.

Our approach allowed us to evaluate precisely conditions needed for an introduction of silicon into the metallic phase. As the empirical activity-composition models found in literature are not consistent with thermodynamics we have developed an improved activity-compositions model compatible with general thermodynamics relations. The results obtained for the Mg-Fe-Si system are in agreement with previous observations, e.g., Nitsan (1974). The only discrepancies are found at low temperatures. Here, more experimental works are needed in order to compare computed equilibrium stability limits and those observed experimentally and possibly affected by kinetic processes.

For systems containing nickel we performed a detailed computations in order to precisely evaluate its influence to the stability limits. We found that for a mantle olivine containing nickel as a major impurity (typically about 3000 wtppm) the stability limits can be shifted by about 2 log f_{O_2} units to more oxidizing conditions. A similar trends was found for the simplified model of mantle peridotite. This fact has important implications for mantle properties, such as electrical conductivity, and should be taken into account when performing laboratory experiments.

Acknowledgment

The authors wish to thank Olivier Jaoul for his thoughtful reviews which helped to improve greatly the manuscript and Laurent Richard for a fruitful discussion when predicting thermodynamic values of unknown endmembers.

Appendix

To illustrate how we derived the Margules energies from the metallurgical parameters, we can take the example of an alloy where Fe is the solvent. In this case, the general expression (4) can be expanded as a Taylor series of the quantities x_{Ni} and x_{Si}. Remembering that $x_{Fe} = 1 - x_{Ni} - x_{Si}$, one gets for the activity of Si

$$RT \ln \gamma_{Si}^{Fe} \sim W_{SiFe} + (-4W_{SiFe} + 2W_{FeSi})x_{Si} + (-2W_{SiFe} - 2W_{NiFe} + W_0)x_{Ni}. \tag{A1}$$

However the metallurgic approach (equations (7-8)) implies that

$$RT \ln \gamma_{Si}^{Fe} = \Delta G_{Si}^{Fe} + RT \ln \frac{p_{Si}}{x_{Si}} + RT(e_{Si/Si}^{Fe} p_{Si} + e_{Si/Ni}^{Fe} p_{Ni}), \tag{A2}$$

where

$$p_{Si} = 100 \frac{M_{Si} x_{Si}}{M_{Si} x_{Si} + M_{Ni} x_{Ni} + M_{Fe} x_{Fe}}, \qquad p_{Ni} = 100 \frac{M_{Ni} x_{Ni}}{M_{Si} x_{Si} + M_{Ni} x_{Ni} + M_{Fe} x_{Fe}}, \tag{A3}$$

and M_i is the molar mass of element i. This last equation has the Taylor expansion

$$\begin{aligned} RT \ln \gamma_{Si}^{Fe} \sim{}& \Delta G_{Si}^{Fe} + RT \ln(100 \frac{M_{Si}}{M_{Fe}}) + \\ & RT(100 \frac{M_{Si}}{M_{Fe}} e_{Si/Si}^{Fe} - \frac{M_{Si} - M_{Fe}}{M_{Fe}}) x_{Si} + RT(100 \frac{M_{Ni}}{M_{Fe}} e_{Si/Ni}^{Fe} - \frac{M_{Ni} - M_{Fe}}{M_{Fe}}) x_{Ni} \end{aligned} \tag{A4}$$

By identification of (A1) and (A4), we derive that

$$W_{SiFe} = \Delta G_{Si}^{Fe} + RT \ln(100 \frac{M_{Si}}{M_{Fe}}), \tag{A5}$$

$$-4W_{SiFe} + 2W_{FeSi} = RT(100 \frac{M_{Si}}{M_{Fe}} e_{Si/Si}^{Fe} - \frac{M_{Si} - M_{Fe}}{M_{Fe}}), \tag{A6}$$

$$-2W_{SiFe} - 2W_{NiFe} + W_0 = RT(100 \frac{M_{Ni}}{M_{Fe}} e_{Si/Ni}^{Fe} - \frac{M_{Ni} - M_{Fe}}{M_{Fe}}). \tag{A7}$$

Similarly, other relationships between W_{ij} and $e^k i/j$ are found by identifying the expressions for γ_{Ni}^{Fe} and γ_{Si}^{Ni} deduced from the Margules expansion with those used in metallurgy. The empirical

models, for Ni and Si diluted in Fe (Rist et al. 1974), and for Fe and Si diluted in Ni (Witzke and Gatellier 1996), include 9 parameters: 3 dissolution enthalpies (Table 2b) and 6 interaction coefficients (Table 2c). However, only 7 independent parameters are required in the expression (4). This indicates that the empirical parameters are not independent and that 2 'observations' could have been theoretically predicted. Indeed we can show the following relations between the interaction coefficients and dissolution enthalpies :

$$e^{Fe}_{Ni/Si} = e^{Fe}_{Si/Ni}\frac{M_{Ni}}{M_{Si}} + \frac{M_{Ni} - M_{Si}}{100\ M_{Si}}, \tag{A8}$$

$$\Delta G^{Fe}_{Ni} = RT\left(\frac{M_{Ni}(1 - 100\ e^{Fe}_{Ni/Ni})}{3M_{Fe}} - \ln(100\ \frac{M_{Ni}}{M_{Fe}}) + \frac{M_{Fe}(1 - 100\ e^{Ni}_{Fe/Fe})}{M_{Ni}} - \frac{1}{2}\right). \tag{A9}$$

The fact that the observations data closely verify these two equations is a striking confirmation of the validity of Margules' approach.

References

Arculus R, Holmes R, Powell R, Righter K (1990) Metal-silicate equilibria and core formation In: Newsom H, Jones J (eds) Origin of the Earth. Oxford University Press, pp 251–271

Boland J, Duba A (1981) Solid state reduction of iron in olivine, planetary and metallic evolution Nature 294:142–144

Boland J, Duba A (1986) Electron microscopy study of the stability field and degree of nonstoichiometry in olivine Journal of Geophysical Research 91:4711–4722

Bowen N, Schairer J (1935) The system $MgO - FeO - SiO_2$ American Journal of Science 29:151

Chart T (1970) A critical assessment of the thermodynamic properties of the system iron-silicon High Temperature and High Pressure 2:461–470

Ehlers K, Grove T, Sisson T, Recca S, Zervas D (1992) The efeect of oxygen fugacity on the partitioning of nickel and cobalt between olivine, silicate melt, and metal Geochimica and Cosmochimica Acta 56:3733–3743

Fei Y, Mao H.-K, Mysen B (1991) Experimental determination of element partitioning and calculation of phase relations in the $MgO - FeO - SiO_2$ system at high pressures and high temperatures Journal of Geophysical Research 96:2157–2169

for the Promotion of Science T. J. S (1988) Steelmaking Data Sourcebook. Gordon and Breach Science Publishers

Gaskell D (1981) Introduction to Metallurgical Thermodynamics. Hemisphere Publishing Corporation

Guillermet A, Gustafson P (1985) An assessment of the thermodynamic properties and the (p, T) phase diagram of iron High Temperature and High Pressure 16:591–610

Guyot F, Zhang J, Martinez I, Matas J, Ricard Y, Javoy M (1997) Pvt measurements of fersilicite (ϵ-fesi). implications for silicate-metal interactions in the early earth Earth and Planetary Science Letters 9:277–285

Hart S, Zindler A (1986) In search of a bulk earth composition Chemical Geology 57:247–267

Helffrich G, Wood B (1989) Subregular model for multicomponent solutions American Mineralogist 74:1016–1022

Helgeson H, Delany J, Nesbitt H, Bird D (1978) Summary and critique of the thermodynamic properties of rock-forming minerals American Journal of Science 278-A:1–229

Holmes R, O'Neill H, Arculus R (1986) Standard gibbs free energy of formation for Cu_2O, NiO, CoO and Fe_xO: High resolution electrochemical measurements using zirconia solid electrolytes from 900-1400 K Geochimica et Cosmochimica Acta 50:2439–2452

Jones J, Drake M (1986) Geochemical constraints on core formation in the earth Nature 322:221–228

Koch-Muller M, Cemic L, Langer K (1992) Experimental and thermodynamic study of $Fe - Mg$ exchange between olivine and ortho-pyroxene in the system $MgO - FeO - SiO_2$ European Journal of Mineralogy 4:115–135

Lemelle L, Guyot F, Leroux G, Libourel G (1999) Mechanism of precipitation of (Fe, Ni) alloy in olivine single crystals under reducing conditions Geochimica et Cosmochimica Acta:submitted

McCoy C, Kolek A, Langenberg F (1967) Application of thermodynamic data during stainless steel melting In: Fitterer G (ed) Applications of fundamental thermodynamics to metallurgical processes. Gordon and Breach Science Publishers, pp 249–280

Nakamura A, Schmalried H (1983) On the nonstoichiometry and point defects of olivine Physics and Chemistry of Minerals 10:27–37

Nash P, Nash A (1991) Nickel-silicon In: Nash P (ed) Phase Diagrams of Binary Nickel Alloys. The Materials Information Society, pp 299–306

Navrotsky A (1994) Thermochemistry of crystalline and amorphous silica In: Heaney P (ed) Silica, Physical Behaviour, Geochemistry and Materials applications. Mineralogical Society of America, pp 309–329

Nitsan U (1974) Stability field of olivine with respect to oxidation and reduction Journal of Geophysical Research 79:706–711

O'Neill H (1991) The origin of the moon and the early history of the earth - a chemical model. part2: The earth Geochimimica et Cosmochimica Acta 55:1159–1172

Raghavan V (1989) Phase diagrams of ternary iron alloys. Ternary Systems Containing Iron and Oxygen. Part 5. The Indian Institute of Metals

Rist A, Ancey-Moret M, Gatellier C, Riboud P (1974) Equilibre thermodynamique dans l'élaboration de la fonte et de l'acier Techniques de l'Ingénieur:M1730–M1733

Robie R, Hemingway B, Fisher J (1979) Thermodynamic properties of minerals and related substances at 298.15 K and 1 bar (10^5 pascals) pressure and at higher temperatures Geological Survey Bulletin 1452

Robie R, Hemingway B, Ito J, Krupka K (1984) Heat capacity and entropy of Ni_2SiO_4-olivine from 5 to 1000 K and heat capacity of Co_2SiO_4 from 360 to 1000 K American Mineralogist 69:1096–1101

Saxena S, Chatterjee N, Fei Y, Shen G (1993) Thermodynamic Data on Oxides and Silicates. Springer-Verlag

Schwerdtfeger V, Engell H.-J (1964) Die freie bildungsenthalpie von siliziumdioxid und die aktivitaten von silizium in flussigem eisen und kobalt Archiv fur das Eisenhuttenwesen 6:533–540

Siefert S, O'Neill H (1987) Experimental determination of activity-composition relations in $Ni_2SiO_4 - Mg_2SiO_4$ and $Co_2SiO_4 - Mg_2SiO_4$ olivine solid solutions at 1200 K and 0.1 MPa and 1573 K and 0.5 GPa Geochimica et Cosmochimica Acta 51:97–104

Smith D (1971) Stability of the assemblage iron-rich orthopyroxene-olivine-quartz American Journal of Science 271:370–381

Smith W, Missen R (1991) Chemical Reaction Equilibrium Analysis: Theory and Algorithms. Krieger Publishing Company

Spear F (1993) Methamorphic Phase Equlibria and Pressure-Temperature-Time Paths. Mineralogical Society of America

Sverjensky D (1984) Prediction of gibbs free energies of calcite-type carbonates and the equilibrium distribution of trace elements between carbonates and aqueous solutions Geochimica and Cosmochimica Acta 48:1127–1134

Witzke S, Gatellier C (1996) Contrôle des éléments résiduels dans les alliages Fe – Ni, exemples de l'aluminium et du soufre In: Béranger G (ed) Les alliages de fer et de nickel. pp 163–176

Wood B, Strens R (1971) The orthopyroxene geobarometer Earth and Planetary Science Letters 11:1–6

Table 1a. Thermodynamic parameters used for endmembers

	Enthalpy ΔH_0 kJ/mol	Entropy S_0 J/K/mol	Ref.
Mg_2SiO_4	-2174.320	94.110	1
Fe_2SiO_4	-1478.670*	151.000	1
Ni_2SiO_4	-1396.500	128.100	2
$MgSiO_3$	-1546.290	66.270	3
$FeSiO_3$	-1194.700*	94.560	1
$NiSiO_3$	-1157.525	76.541	P
MgO	-601.490	26.940	1
FeO	-267.270	57.590	1
NiO	-240.110	37.991	4
Fe (bcc)	see ref.	see ref.	7
Fe (fcc)	see ref.	see ref.	7
Ni	0	29.873	4
Si	0	18.810	6
SiO_2 (α)	-910.700	41.460	3
SiO_2 (β)	-910.497	41.700	3
SiO_2 (cristobalite)	-908.864*	43.363	5
O_2	0	205.150	6

* corrected values, see discussion in the text

[1] Fei et al. (1991)
[2] Robie et al. (1984)
[3] Saxena et al. (1993)
[4] Holmes et al. (1986)
[5] Navrotsky (1994)
[6] Robie et al. (1979)
[7] Guillermet and Gustafson (1985)

^{P} estimations based on the approach developed by Helgeson et al. (1978) and Sverjensky (1984)

Table 1b. Heat capacities of endmembers

$C_P = a + bT + cT^{-2} + dT^2 + eT^{-3} + fT^{-0.5} + gT^{-1}$ in J/K/mol for T in K

	a	b (10^{-3})	c (10^6)	d (10^{-3})	e (10^8)	f (10^2)	g (10^3)	T-range
[1] Mg_2SiO_4	166.9983	15.6360	-11.1490	0.0	17.6538	0.0	1.92	
[1] Fe_2SiO_4	167.0023	27.1180	-1.3124	0.0	-2.5649	0.0	-5.56	
[2] Ni_2SiO_4	34.8605	15.8753	10.0776	0.0	0.0	88.81	-164.98	
[3] $MgSiO_3$	144.4500	18.8200	-1.3500	0.0	4.6120	0.0	19.38	
[1] $FeSiO_3$	131.8945	0.0620	-4.9472	0.0	0.1422	0.0	2.3191	
[1] MgO	49.6558	3.8410	-1.3899	0.0	1.2721	0.0	-0.7917	
[1] FeO	68.4368	1.1940	1.6971	0.0	1.3479	0.0	-11.88	
[4] NiO	-27.5520	169.0400	1.9083	0.0	0.0	0.0	0.0	298-525
	-37.7150	175.7300	0.0	0.0	0.0	0.0	0.0	525-565
	58.4170	-7.1210	0.0	0.0	0.0	0.0	0.0	565-800
	35.1090	15.1063	3.9426	0.0	0.0	0.0	0.0	800-1200
	41.5180	12.0380	0.0	0.0	0.0	0.0	0.0	1200-2000
[4] Ni	11.1100	37.8720	0.3228	0.0	0.0	0.0	0.0	298-600
	-2254.1560	2535.0300	276.4775	0.0	0.0	0.0	0.0	600-631
	-70.7540	90.9240	18.5720	0.0	0.0	0.0	0.0	631-700
	20.6880	9.9716	1.5223	0.0	0.0	0.0	0.0	700-1728
[5] Si	31.7780	0.5388	-0.1465	0.0	0.0	-1.79	0.0	298-1685
[3] SiO_2	81.1447	0.1828	-0.1810	5405.80	0.0	-6.98	0.0	298-848
(alpha)	75.8210	1.2050	1.7310	0.0	1.2020	0.0	-12.13	848-
[3] SiO_2	81.1447	0.1828	-0.1810	5405.80	0.0	-6.98	0.0	298-848
(beta)	78.8120	1.2050	1.7310	0.0	1.2020	0.0	-12.13	848-
[3] SiO_2	-1399.8908	5715.8000	26.2880	-6.2446	0.0	0.0	0.0	298-373
(crist)	2178.3561	-6987.2000	-58.2010	6.4573	0.0	0.0	0.0	373-453
	7860.2125	-23634.000	-255.0100	20.1910	0.0	0.0	0.0	453-543
	77.5875	-6.0805	-4.4542	2778.70	0.0	0.0	0.0	543-3300
[5] O_2	48.3130	-0.6913	0.4992	0.0	0.0	-4.21	0.0	

[1] Fei et al. (1991) [2] Robie et al. (1984) [3] Saxena et al. (1993)
[4] Holmes et al. (1986) [5] Robie et al. (1979)

Table 2a. Margules parameters

in olivine and pyroxene (kJ/mol)

W^{ol}_{MgFe}	7.12±1.8	1
W^{ol}_{FeNi}	0.35±1.0	2
W^{ol}_{MgNi}	0.35±1.0	2
W^{px}_{MgFe}	3.42±2.1	1
W^{px}_{FeNi}	0.0±	3
W^{px}_{MgNi}	0.0±	3

[1] Koch-Muller et al. (1992)

[2] Siefert and O'Neill (1987)

[3] O'Neill (1991)

Table 2b. Enthalpies of dissolution

in metal (kJ/mol) at T=1873 K

ΔG^{Fe}_{Ni}=−76.077
ΔG^{Fe}_{Si}=−157.932
ΔG^{Si}_{Ni}=−215.135

Table 2c. Coefficients of interaction $e^k_{i/j}$ in metal

e^{Fe}_{SiSi}	0.2533	1
e^{Fe}_{SiNi}	0.0115	1
e^{Fe}_{NiSi}	0.0131	1
e^{Fe}_{NiNi}	0.0021	1
e^{Ni}_{SiSi}	0.2533	2
e^{Ni}_{FeFe}	0.0299	2

[1] Rist et al. (1974)

[2] Witzke and Gatellier (1996)

Table 2d. Margules parameters in metal at different temperatures in (kJ/mol) and their temperature derivatives (J/mol/K)

	T=1873 K	T=1573 K	T=1273 K	$\frac{dW_{ij}}{dT}$
W_{SiFe}	-98.425	-103.683	-108.941	17.53
W_{NiFe}	-8.267	-7.090	-5.913	-3.92
W_{SiNi}	-159.634	-155.088	-150.542	-15.16
W_{FeNi}	-15.375	-13.030	-10.684	-7.82
W_{FeSi}	-93.799	-120.821	-147.842	90.07
W_{NiSi}	-220.862	-227.532	-234.201	22.24
W_0	-195.352	-206.402	-217.452	36.83

Figure 1: Activities of Fe (a), Ni (b), and Si (c) in the ternary alloy Fe-Ni-Si. In each triangle, the Fe, Si and Ni contents are 100% in the bottom left, top and bottom right corners, respectively. The curvature of the isoactivity lines is the expression of the strong non-ideality of the solution. The isolines correspond to values of activities between 0.1 and 0.9.

Figure 2: Stability curves of the OSI (a) and PSI (b) equilibria. The horizontal axis depicts the temperature in 10^4/K units (bottom) or K units (top), the vertical axis corresponds to the oxygen fugacity in bars. The thickness of the stability curves (shaded areas) are due to uncertainties in the thermodynamic data. The dashed lines were obtained by Nitsan (1974). The stable phases of silica, silicon, iron and silicates are indicated as a function of temperature.

Figure 3: Stability curves of olivines (a) and pyroxene (b) in the (T-f_{O_2}) space for three Mg/(Mg+Fe) ratios (99% for Fa1 and Fs1, 90% for Fa10 and Fs10, and 0% for Fa100 and Fs100). The widths of the shaded areas are due to the thermodynamic uncertainties. Neglecting the non-ideality of the mixing would shift the stability fields towards more reducing conditions for the olivines, dashed lines in (a). The effects of non-ideality are negligible in pyroxenes.

Figure 4: Difference between the stability curves of OPI and OSI as a function of temperature. A negative f_{O_2} (left axis) or a silica activity less than 1 (right axis) indicates that olivine is reduced to pyroxene and metal (e.g. Fa10). Although uncertainties are large, our model suggests that pure fayalite reduces to silica+iron whereas magnesium rich fayalite reduces to pyroxene+metal.

Figure 5: Molar fraction of silicon in the metallic phase in equilibrium with silicates for three Mg/(Mg+Fe) ratios (99% for Fa1 and Fs1, 90% for Fa10 and Fs10, and 0% for Fa100 and Fs100). The silicon content in the alloy increases when the Fe/(Fe+Mg) ratio in olivine (a) and in pyroxene

(b) decreases. The widths of shaded areas are related to the thermodynamic uncertainties.

Figure 6: Stability limit of San-Carlos olivine with respect to metal precipitation. The presence of 3000 wtppm of Ni_2SiO_4 shifts the stability limit to less reducing conditions than for pure Mg-Fe olivine (Fa10).

Figure 7: Nickel molar fraction in the metallic phase in equilibrium with mantle olivine (3000 ppm of Ni_2SiO_4). The nickel fraction decreases at high temperature.

Figure 8: Compositions of metallic phase (a), olivine (b) and pyroxene (c) as a function of oxygen fugacity for a temperature of 1700 K. Ni, Fe and Si are successively exsolved from the silicate phases as the conditions become more reducing. In (a) the dotted lines are obtained when simplified activity-composition relationships are used.

Figure 9: Stability limit of simplified peridotite (dark shading) compared to those of mantle olivine and Fa10 (light shading).

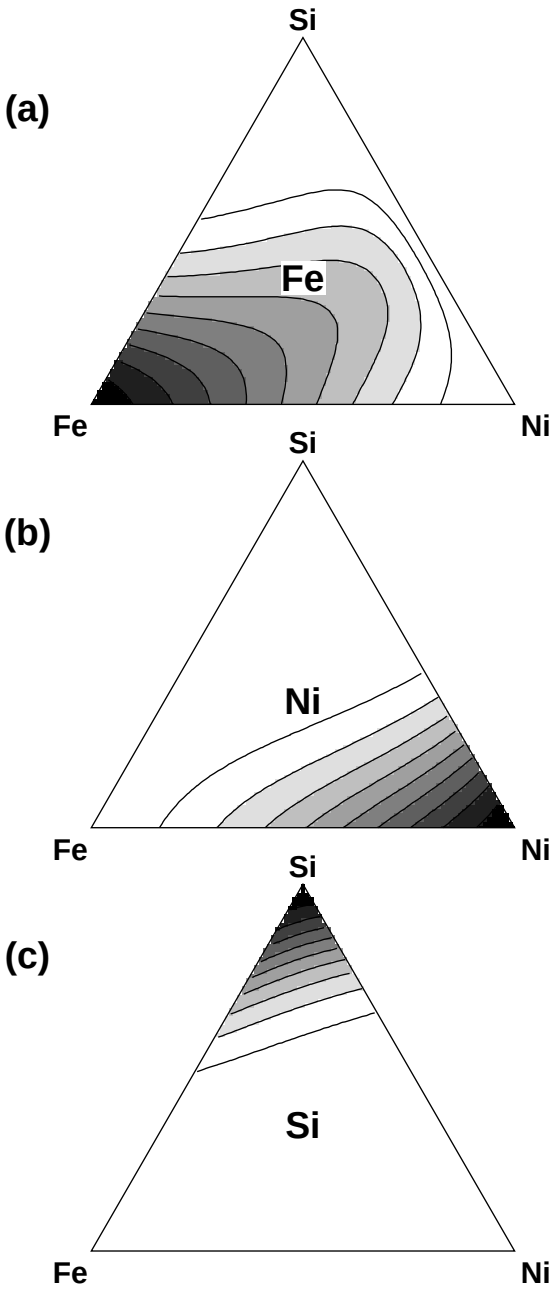
(a)
Si
Fe
Fe
Ni
(b)
Si
Ni
Fe
Ni
(c)
Si
Si
Fe
Ni

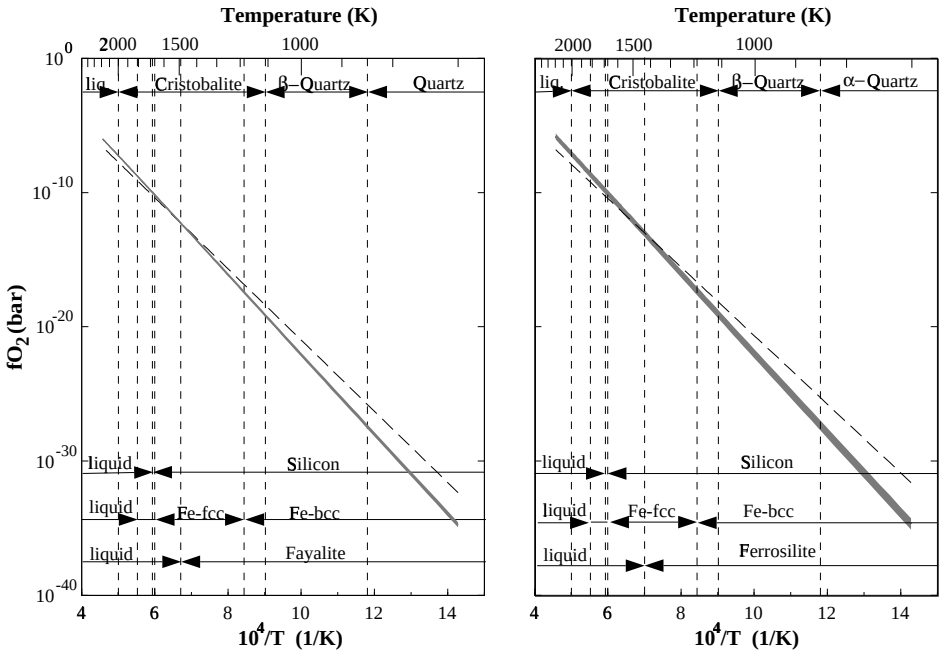
Temperature (K)
2000
1500
1000
liq.
Cristobalite
β−Quartz
Quartz
α−Quartz
liquid
Silicon
Fe-fcc
Fe-bcc
Fayalite
Ferrosilite
fO_2 (bar)
10^{4}/T (1/K)

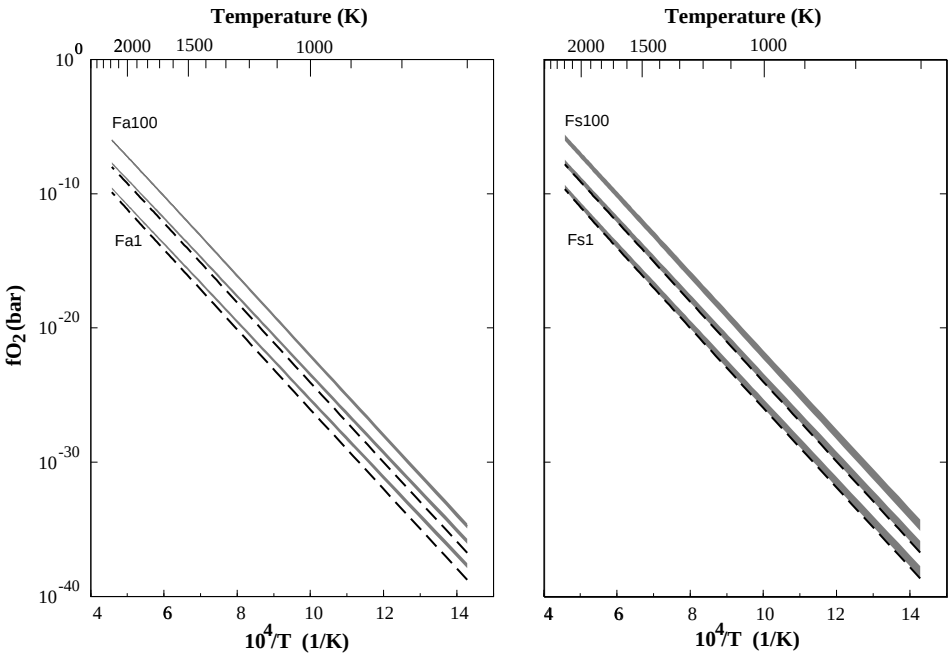
Temperature (K)
2000
1500
1000
10^{0}
10^{-10}
10^{-20}
10^{-30}
10^{-40}
Fa100
Fa1
fO_2(bar)
4
6
8
10
12
14
10^4/T (1/K)
Temperature (K)
2000
1500
1000
Fs100
Fs1
4
6
8
10
12
14
10^4/T (1/K)

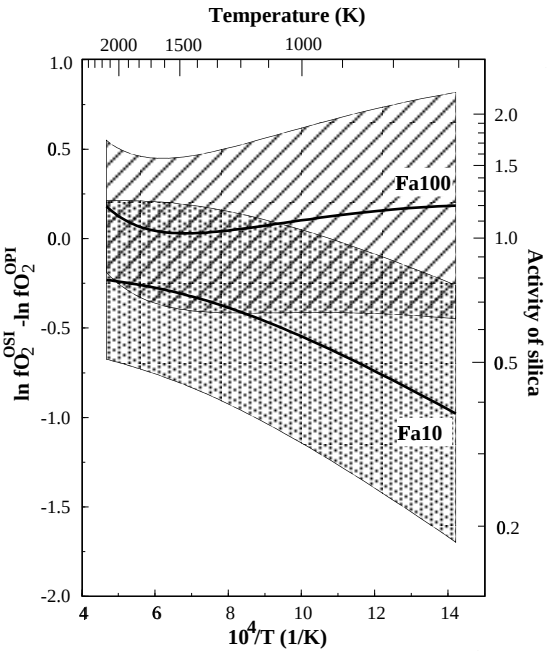
Temperature (K)
2000
1500
1000
1.0
0.5
0.0
-0.5
-1.0
-1.5
-2.0
2.0
1.5
1.0
0.5
0.2
Fa100
Fa10
ln fO2OSI -ln fO2OPI
Activity of silica
4
6
8
10
12
14
10^4/T (1/K)

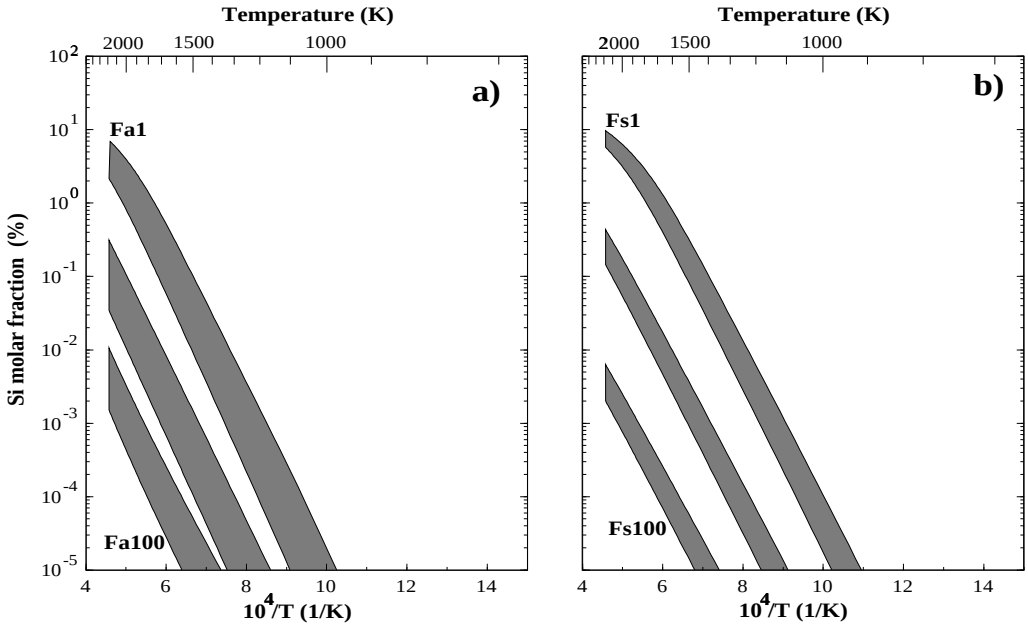
Temperature (K)
2000
1500
1000
a)
Fa1
Fa100
Si molar fraction (%)
10^{2}
10^{1}
10^{0}
10^{-1}
10^{-2}
10^{-3}
10^{-4}
10^{-5}
4
6
8
10
12
14
10^{4}/T (1/K)
Temperature (K)
2000
1500
1000
b)
Fs1
Fs100
4
6
8
10
12
14
10^{4}/T (1/K)

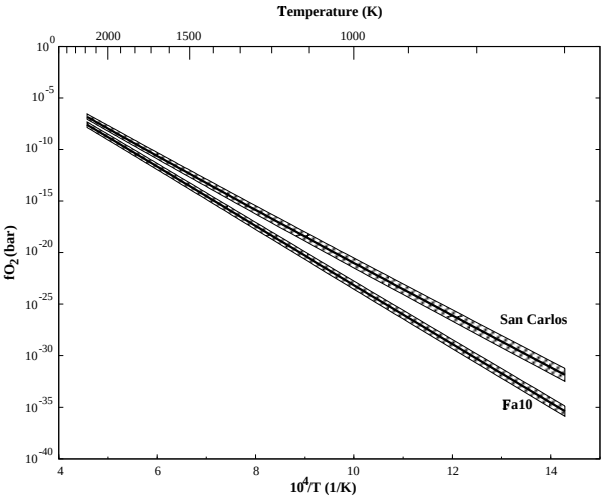
Temperature (K)
2000
1500
1000
10^{0}
10^{-5}
10^{-10}
10^{-15}
10^{-20}
10^{-25}
10^{-30}
10^{-35}
10^{-40}
fO_2(bar)
San Carlos
Fa10
4
6
8
10
12
14
10^4/T (1/K)

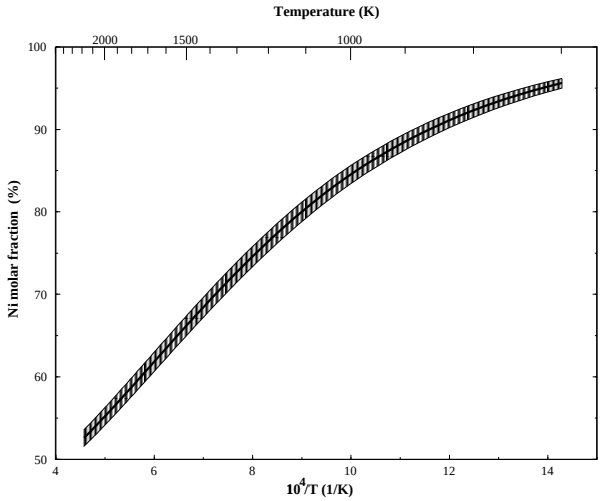
Temperature (K)
2000
1500
1000
100
90
80
70
60
50
Ni molar fraction (%)
4
6
8
10
12
14
10^4/T (1/K)

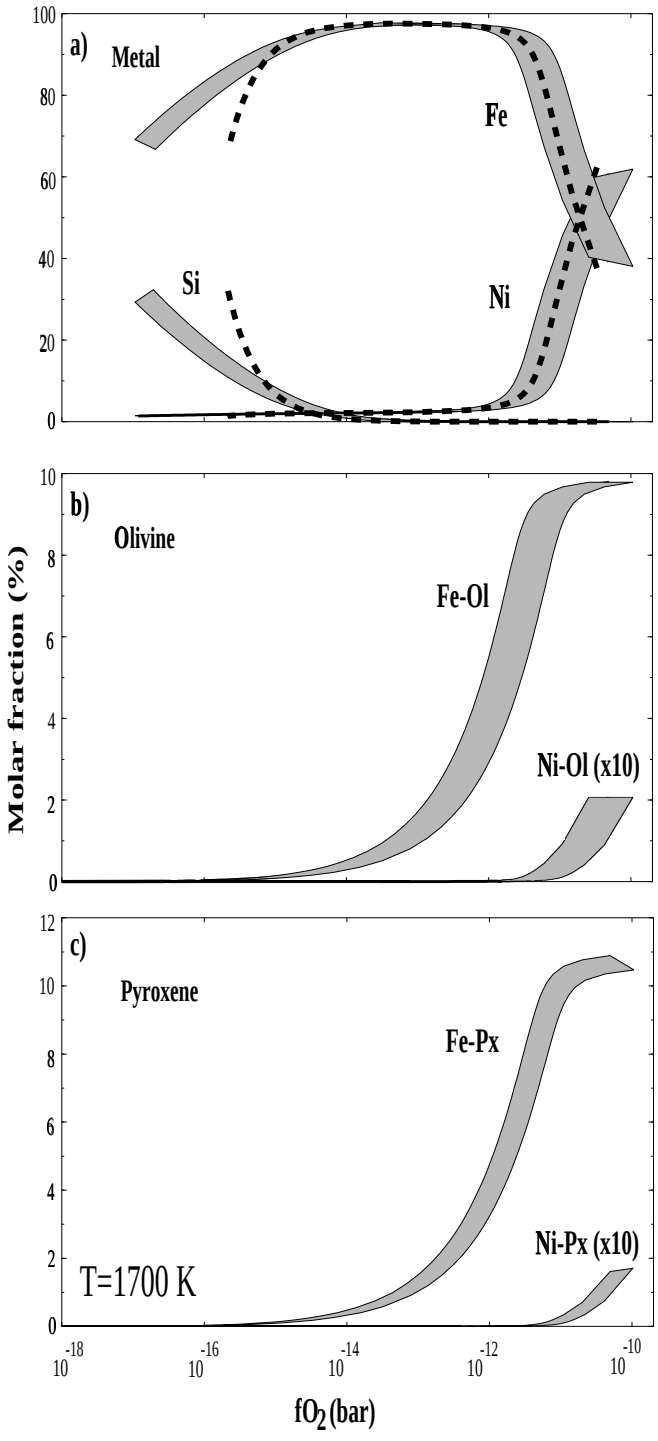
a)
Metal
Fe
Si
Ni
b)
Olivine
Fe-Ol
Ni-Ol (x10)
c)
Pyroxene
Fe-Px
Ni-Px (x10)
T=1700 K
Molar fraction (%)
fO2 (bar)

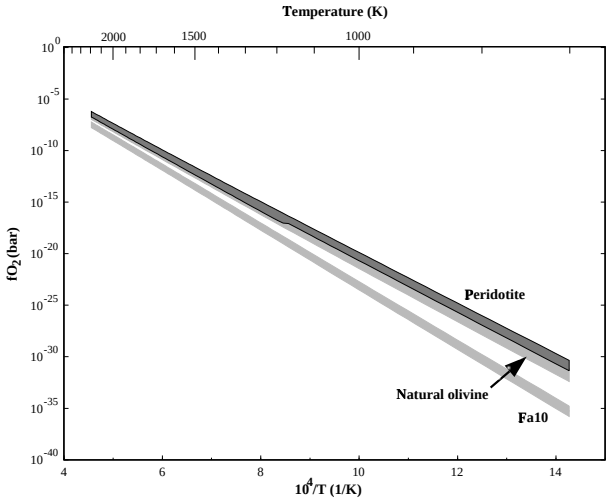
Temperature (K)
2000
1500
1000
10^{0}
10^{-5}
10^{-10}
10^{-15}
10^{-20}
10^{-25}
10^{-30}
10^{-35}
10^{-40}
fO_2 (bar)
Peridotite
Natural olivine
Fa10
4
6
8
10
12
14
10^4/T (1/K)